This project has received funding from the European Union's Horizon 2020 research and innovation programme under grant agreement No 727616.

Biofficiency

Fly ash formation model for biofuels

(D5.3)

Author:	Flemming J. Frandsen
Version:	Final
Quality Review:	Sebastian Fendt
Date:	18.10.2019
Partners involved:	DTU, TUM

Grant Agreement No.	727616
Starting Date:	01.11.2016
Duration:	36 months

Disclaimer

The content of this deliverable does not reflect the official opinion of the European Commission. Responsibility for the information and views expressed herein lies entirely with the author(s).

Table of Contents

Abbreviations and Acronyms iii
1. Introduction 1
2. A Simple Model for Fly Ash Formation in PF-Units 2
2.1. Concentration of Gases and Aerosols 3
2.1.1. Release of K, Cl and S 3
2.1.2. Gas Phase Reactions 5
2.1.3. Aerosol Formation 7
2.2. Coarse Ash Fraction 7
2.2.1. Fly Ash Particle Size Distribution 7
2.2.2. Rosin-Rammler Parameters 8
2.2.3. Ash Median Particle Size 10
2.2.4. Final Model for Ash PSD 11
2.2.5. Chemistry of the Coarse Ash Fraction 12
3. Simulations of Aerosol and Fly Ash Formation 13
3.1. Release of K,S and Cl: Freeboard Chemistry 13
3.2. Aerosol Formation 14
3.3. Coarse Fly Ash Formation 14
4. Summary and Conclusion 17
References 19

Abbreviations and Acronyms

EFR	Entrained flow reactor
PF	Pulverised fuel
PSD	Particle Size Distribution
RR	Rosin-Rammler
XRD	X-Ray diffraction

1. Introduction

The ash formation mechanism in pulverized fuel combustion has been well-established, indicating that ash particles generated during pulverized fuel combustion primarily originate from excluded minerals, included minerals and organically associated ash forming species in the fuel particles, see Figure 1.

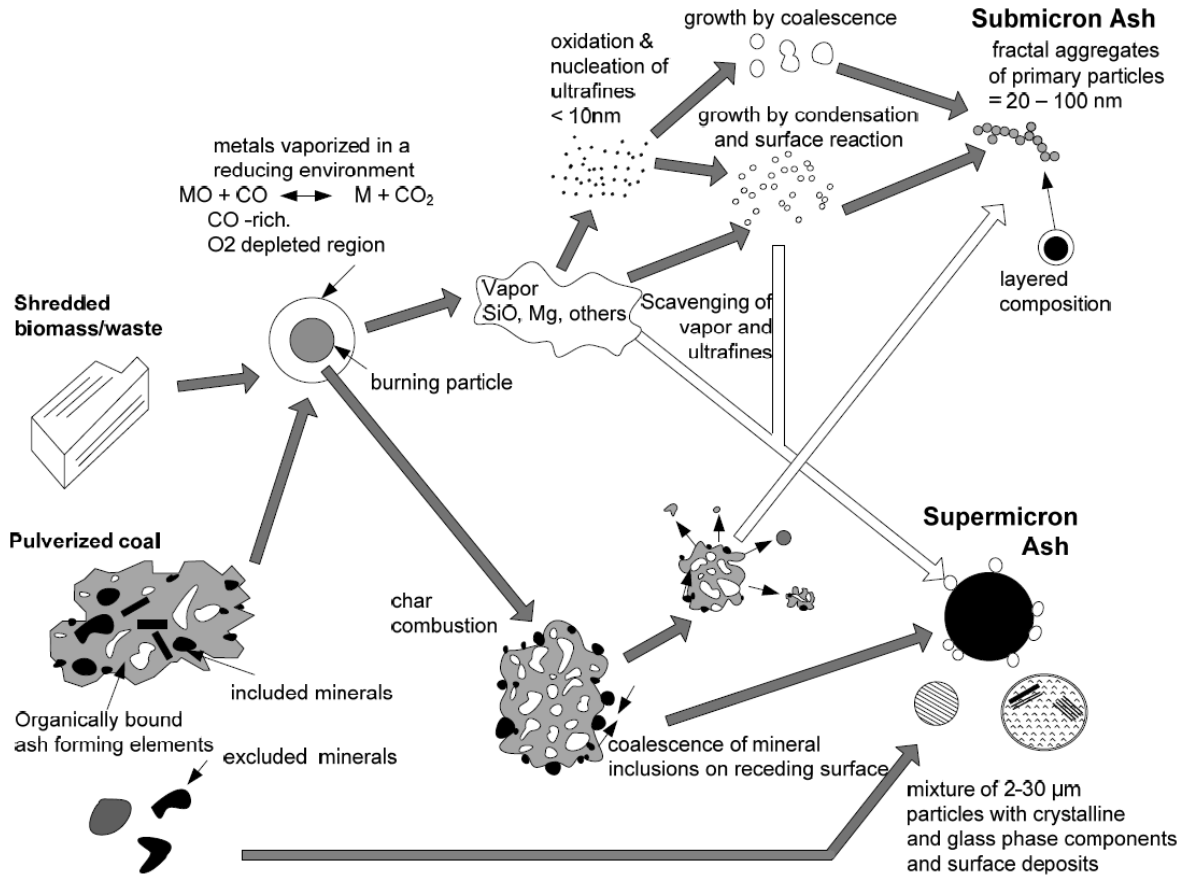

Figure 1: Ash formation pathways during solid fuel combustion. Adapted from [Lighty et al., 2000].

When pulverized fuel particles are combusted, a fraction of the included minerals and organically associated ash-forming elements are released to gas phase, either through a direct release mechanism, or, a mechanism involving reducing reactions. After that, the vaporized inorganic elements may nucleate to ultrafine particles, condense on the surface of existing particles, or chemically react with other particles. The partitioning of the vaporized inorganic elements, is dependent on the fuel properties and the combustion conditions, such as cooling rate and particle density in the flue gas [Frandsen, 2017]. The ultrafine particles generated from the nucleation of inorganic vapors may aggregate/coalesce with themselves to form larger particles, which are usually an important source of submicron ash particles, formed during pulverized fuel combustion. On the other hand, the ultrafine particles may also attach to the surface of the existing large fly ash particles, which may therefore partition to the supermicron ash particles [Frandsen, 2017].

In addition to the fraction that is vaporized, the remaining minerals and organically associated ash forming elements in the fuel particles may undergo fragmentation, melting and coalescence during the fuel conversion process. The majority of these ash-forming elements

cause formation of super micron ash particles, while a small fraction may contribute to the formation of submicron ash particles, probably via the fragmentation mechanism. The excluded minerals may also experience melting and a minor extent of fragmentation/coalescence (depending on the mineral type), and may be converted mainly to super micron ash particles during the combustion process [Frandsen, 2017].

Below, is a brief outline of a simple model for fly ash formation in PF-units.

2. A Simple Model for Fly Ash Formation in PF-Units

Before a calculation of deposit formation can be initiated, a proper description of the ash present in the flue gas is needed. During the combustion, the inorganic matter (ash) in a fuel particle can roughly be divided in two parts; a vaporized fraction and a coarse fraction, see Figure 2.

The vaporized part (K, Cl and S) may then react and nucleate forming gaseous components and aerosols, while the coarse fraction of the ash can be described by a particle size distribution and by the chemistry of the particles.

Then, by knowing the chemistry and the temperature of the particles, material properties can be predicted. Part of the coarse ash will be found as large particles, which are unable to follow the flue gas up through the furnace and will be 'lost' primarily as bottom ash [Hansen et al., 2017a,b].

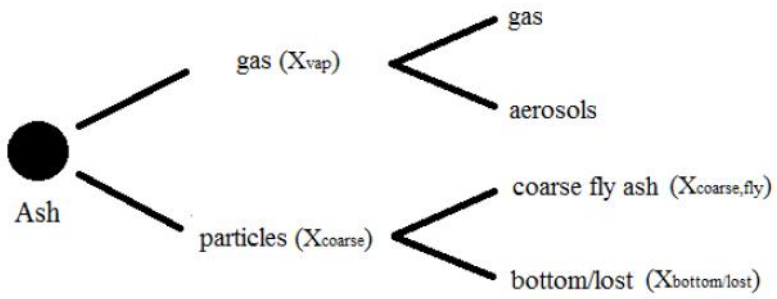

Figure 2: Ash mass balance for the model presented below [Hansen et al., 2017a,b].

A proper model of the fly ash should therefore include species formulation and concentrations of gases, aerosols and coarse ash, and, a particle size distribution of at least the coarse ash fraction. Below, a model for the ash formation, considering these parameters, is briefly outlined.

It is assumed that no interaction occur between the coarse ash particles and the vaporized species in the flue gas, and that part of the large (residual) fly ash fraction is lost in the furnace. All gases and aerosols are thus assumed to follow the flue gas.

An ash mass balance can then be expressed as [Hansen et al., 2017a,b]:

$$1 = X_{vap} + X_{Coarse,fly} + X_{bottom/lost} \quad [1]$$

Where X_{vap} is the vaporized fraction of the fuel ash (forming gases and aerosols). This fraction is estimated in the model, below, based on experimental data. $X_{Coarse,fly}$ is the fraction of the ash found as coarse ash which follows the flue gas. This fraction is determined by either measurements or assumptions.

2.1. Concentration of Gases and Aerosols

The description of gas and aerosol concentrations occur in three consecutive steps, in the model;

- First, the vaporized fraction (X_{vap}) is calculated, by assumptions on release of the individual elements; K, Cl and S.
- Then, reaction between the elements forming KCl, KOH, K_2SO_4, SO_2 and HCl is described.
- Finally, physical transformations of the individual species into aerosols are proposed.

These steps are outlined below.

2.1.1. Release of K, Cl and S

The release of inorganic elements to the gas phase has been examined e.g. by entrained flow reactor (EFR) combustion tests with various woods and straws along with olive residue by [Shah et al., 2010] and [Damoe et al., 2014]. These tests were discussed by [Hansen, 2015].

In both combustion units, a near complete release of Cl and S was generally observed. However, for some high-Cl fuels (straw and olive residue) used by [Shah et al., 2010], some Cl was retained in the particles. This has not been explored further. In this model, it is assumed that the fuels experience a full release of S and Cl to the gas phase.

The release of K was generally observed to be above 85 %, in both sets of EFR experiments [Shah et al., 2010; Damoe et al., 2014]. However, for some straws and for the olive residue, a lower release (45-75 %) was observed, probably due to high contents of Si and low content of Ca in the fuels. Thus, retaining effects of Si on the release of K may be important, when Ca is not present in high amounts in the fuel. This has been explored further, as the behavior of K in the combustion, is considered important for the ash deposition behavior.

The release of K as measured by [Shah et al., 2010] and [Damoe et al., 2014] is shown as function of selected molar ratios of the fuels, in Figure 3.

It is seen in Figure 3, that when the molar ratio (Ca+Mg)/Si > 0,5 (at which all Si may be found in relation with Ca or Mg), the release of K was > 85 %. In the model, it is therefore assumed that when the molar ratio (Ca+Mg)/Si > 0.5, the release of K is 90 %.

At lower molar ratios, (Ca+Mg)/Si < 0,5, some K was retained in the particles, and the release of K is lower. In these cases some Si was available for reaction with K, rather than the preferred reaction with Ca or Mg. In Figure 3, it is indicated that for fuels with (Ca+Mg)/Si < 0.5, the K/Si molar ratio influenced the release of K. There is not enough data to make clear conclusions on how the molar ratios influence the K release at these conditions, however, in the model it is assumed that the release can be described by a function of the K/Si molar ratio

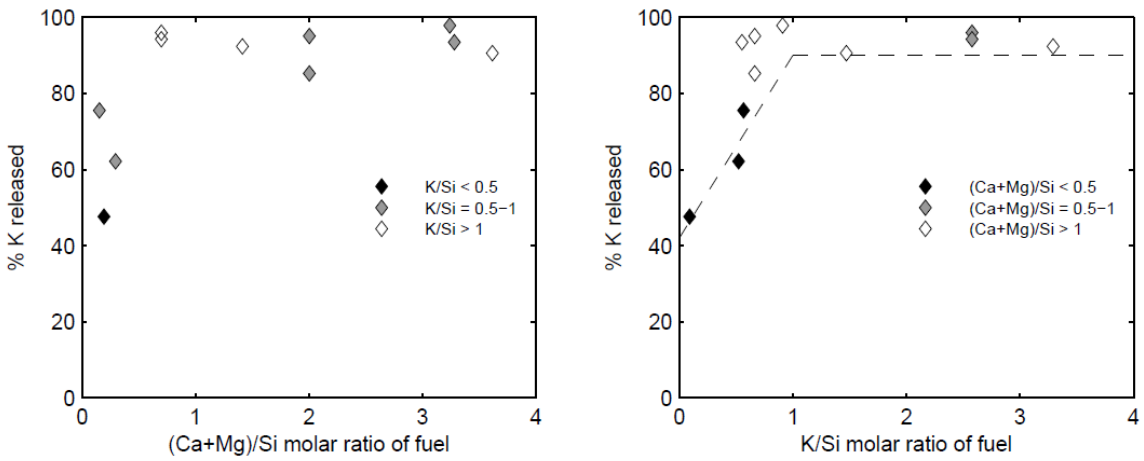

Figure 3: Release of K as function of molar ratios of the fuels. Data from [Shah et al., 2010] and [Damoe et al., 2014]. Fuels considered are 6 woods (bark, wood chips, waste wood, saw dust, wood pellets), 3 straws, and, 1 olive residue.

$$f_{K-release} = \begin{cases} 0{,}9 \; if \; \frac{Ca+Mg}{Si} > 0{,}5 \\ 0{,}9 \; if \; \frac{Ca+Mg}{Si} < 0{,}5 \; and \; \frac{K}{Si} > 1 \\ 0{,}48 \cdot \frac{K}{Si} + 0{,}42 \; if \; \frac{Ca+Mg}{Si} < 0{,}5 \; and \; \frac{K}{Si} < 1 \end{cases} \quad [2]$$

Once $f_{K\text{-release}}$ is determined, the molar flows of the released elements can be calculated.

$$n_{S,vap} = n_{S,fuel}$$

$$n_{Cl,vap} = n_{Cl,fuel}$$

$$n_{K,vap} = f_{K-release} \cdot n_{K,fuel}$$

The inorganic elements introduced with the fuel is given to the model as wt% dry ash in oxide scale, which sum to 100%. The total fraction of vaporized ash from the fuel ash, is calculated from the contents of K_2O, Cl and SO_3 in the fuel ash (recalculated to fractions) [Hansen et al., 2017a,b].

$$X_{vap} = X_{SO3,fuel\ ash} + X_{Cl,fuel\ ash} + f_{K-release} \cdot X_{K2O,fuel\ ash} \quad [3]$$

2.1.2. Gas Phase Reactions

The volatile elements K, Cl and S are released from pulverized fuel particles to the gas phase during combustion. It is expected that Cl is released primarily as KCl(g), K as KCl(g), K(g) or KOH(g) while S is released as SO_2 (g). After release of the elements, sulfation of KCl (or KOH), forming K_2SO_4 occurs. However, full reaction may not occur. At high temperatures, KCl, HCl, K_2SO_4 and SO_2 exist in equilibrium [Hansen et al., 2017a,b]. As the temperature is lowered the HCl/KCl equilibrium moves toward KCl and the K_2SO_4/SO_2 equilibrium is shifted toward K_2SO_4. The latter equilibrium is, however, kinetically hindered by the availability of SO_3, and equilibrium may not be reached within the residence time of a combustion plant. [Christensen et al., 1998] states that reaction mainly occurs until the cooling has reached around 800 °C. At further cooling, only phase transitions occur.

In the model, two scenarios may occur;

- In the EFR, the concentration of SO_2 in the flue gas is usually measured, while;
- In full-scale combustion tests, such gas measurements may be difficult to get.

Thus, the gas phase reactions are modeled in different ways. In the model, only the final state of the gas phase components near the deposit probe is considered, i.e. the form of the elements during the release and reaction pathways to the final form, are not considered.

SO_2 Concentration Measured

In case the SO_2 concentration is known, it is assumed that S in the flue gas, not found as SO_2, will be present as K_2SO_4. The distribution of Cl among KCl and HCl is then subsequently determined, by assuming that the reaction below is in equilibrium, and, by omitting the dimer K_2Cl_2.

$$KCl + H_2O \rightleftharpoons HCl + KOH \quad [4]$$

The concentrations of KCl, KOH and HCl in the flue gas, is determined by solving Equations [5-7], assuming a constant concentration of H_2O. $[K]_{released}$ is the amount of released K, not consumed by SO_2 in formation of K_2SO_4.

$$\frac{[KCl]\cdot[H_2O]}{[KOH]\cdot[HCl]} = K_C \quad [5]$$

$$[KCl] + [HCl] = [Cl]_{released} \quad [6]$$

$$[KCl] + [KOH] = [K]_{released} \quad [7]$$

The equilibrium constant has been derived from a detailed alkali reaction mechanism, proposed by Glarborg and Marshall [125].

$$K_C = 0{,}456 \cdot exp\left(\frac{1{,}35\cdot 10^5}{8{,}314\cdot T}\right) \quad [8]$$

The HCl/KCl-equilibrium is shown as function of temperature for two K/Cl molar ratios, in Figure 4. It is seen that the HCl/KCl equilibrium favors KCl at temperatures up to 900 °C. If K is in excess of Cl, HCl formation is only predicted at high temperatures.

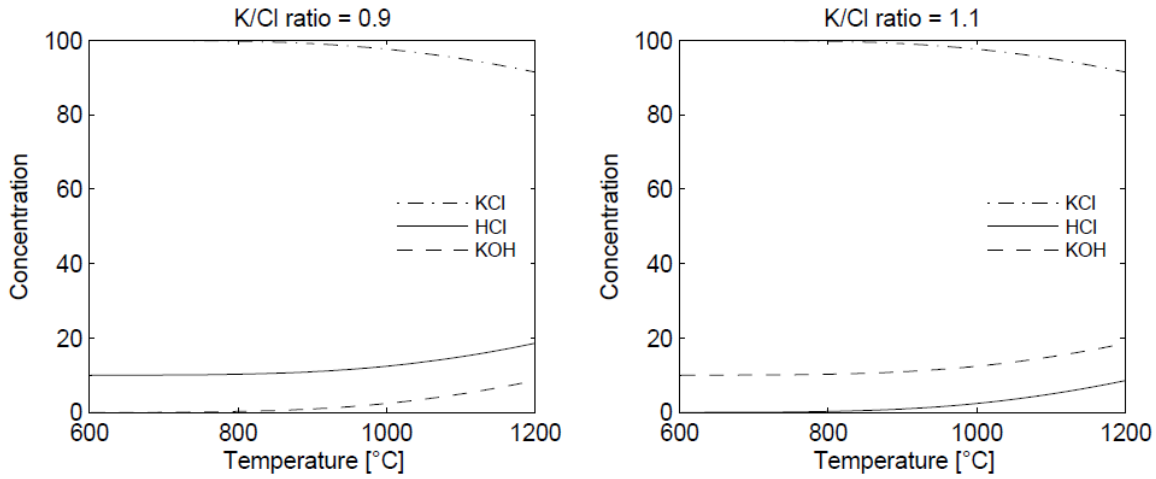

Figure 4: Prediction of KCl, KOH and KCl formation by Equations [5-8]. Left: Cl in excess of K, Right: K in excess of Cl.

No Gas Concentration Measurements

When there is no measurement of the relevant gas phase species available, as in the full-scale experiments, all the gas phase species are assumed to participate in an equilibrium.

If K is present in stoichiometric excess, all S and Cl is found to react with K, and excess K is found as KOH. This observation was made for grate fired boilers [Christensen et al., 1998]. It is assumed that there is enough reaction time, before the probe, for this to occur.

When K is not in stoichiometric excess, formation of SO_2 and HCl will occur. It was found by [Christensen et al., 1998], that in a grate-fired boiler, the species K_2SO_4/SO_2/KCl/HCl are in equilibrium during cooling, when the temperature is above 800 °C. [Christensen et al., 1998] uses these four species in an equilibrium calculation valid for temperatures around 800 °C. At other temperature ranges species like KOH, SO_3, $KHSO_4$, etc. may influence equilibrium. At lower temperatures, the sulfation reaction is kinetically limited [Hansen et al., 2017a,b].

In the model, the equilibrium suggested by [Christensen et al., 1998], with K=0,25, valid at temperatures around 800 °C is applied. by solving Equations [9-12].

$$K_C = \frac{[K_2SO_4]\cdot[HCl]^2}{[SO_2]\cdot[KCl]^2} = 0{,}25 \quad [9]$$

$$[KCl] + 2\cdot[K_2SO_4] = [K]_{released} \quad [10]$$

$$[KCl] + [HCl] = [Cl]_{release} \quad [11]$$

$$[K_2SO_4] + [SO_2] = [S]_{released} \quad [12]$$

The influence of temperature has not been explored further, and is neglected, as the majority of the deposit measurements, are made at temperatures around 700-900 °C.

The estimations of the gas phase reactions presented above are quite simple. It is acknowledged that they are in fact more complicated and influenced by various other factors, such as other gas components like K_2CO_3, and, formation of aerosols which impact the equilibrium. However, it is anticipated that the contribution of these species in the deposit formation are small compared to the deposit formation of the coarse ash. Therefore, these simple estimates are considered adequate [Hansen et al., 2017a,b].

2.1.3. Aerosol Formation

Once the concentrations of KCl, K_2SO_4 and KOH are determined, appearance of the species as gaseous component, or, aerosol is estimated. If the calculated concentrations of the K-species are above their saturation pressure, at the given flue gas temperature near the probe, the presence of aerosols is assumed. The saturation pressure in [bar], is calculated by Equation [13].

$$log_{10}(P_{sat}) = \frac{A \cdot 10^3}{T_{fg}} + B \cdot log_{10}(T_{fg}) + C \quad [13]$$

The constants used in Equation [13] are provided in Table 1. The saturation pressures are then recalculated to saturation concentrations by the ideal gas law. Then, if the calculated concentrations of the K-species are above the saturation concentration, the gas concentration of the K-species is set to the saturation concentration, while the remaining of the K-species will be present as aerosol [Hansen et al., 2017a,b].

The aerosols present in the system, are assumed to have a 0,5 µm diameter based on observations made by [Zheng et al., 2007] and [Nordgren et al., 2013]. The particle size distribution of aerosols, is thus neglected.

Table 1: Constants used in Equation [13]. Source: [Hansen et al., 2017a,b].

Species	Tm [K]		A	B	C
KCl	1045	T<Tm	-12.151	-2.99	17.254
		T>Tm	-11.326	-4.21	20.148
K_2SO_4	1342	T<Tm	-19.286	-7.15	31.895
		T>Tm	-16.549	-5.62	25.071
KOH	679	T<Tm	-10.112	-3.11	16.725
		T>Tm	-9.723	-3.36	16.860

2.2. Coarse Ash Fraction

A very important parameter in modeling of ash deposition, is the particle size distribution of the coarse fly ash. The only measure of particles available from the EFR experiments used for validation of the model are the particle sizes of the fuels - in most cases only provided as a single value, dp_{50}, indicating the median particle size at which 50 % (based on weight or volume) of the particles are below. A link between the dp_{50} of the fuel and a particle size distribution of the fly ash has thus been developed as part of this work. The calculation of the ash PSD is described in the following sections.

2.2.1. Fly Ash Particle Size Distribution

The model describing the particle size distribution of the ash, is based on corresponding samples of fuel and ashes obtained during combustion of straws and woods in an EFR.

Particle size distributions of fuels and ashes can generally be described by a Rosin-Rammler distribution (RR-distribution), which is a continuous probability distribution often applied to coal particles by [Rosin and Rammler, 1933], and, subsequently described in detail by [Weibull, 1951].

The cumulative distribution of particles (F(dp)), can by use of the Rosin-Rammler approach be described by Equation [14], in which two parameters occur. The parameters used are generally referred to as a 'shape' parameter or exponent (n), describing the shape of a distribution (or efficiency of size fractionation), which is relatively constant, and, a 'scale' parameter, λ, which

varies with the overall fineness of the particles in a sample and has units similar to dp, in this case [µm].

$$F(dp) = 1 - exp\left[-\left(\frac{dp}{\lambda}\right)^{n}\right] \quad [14]$$

The parameters of the RR-distribution are connected to the median (or dp_{50}) of the particles, as given by Equation [15].

$$dp_{50} = \lambda \cdot (\ln(2))^{1/n} \quad [15]$$

Thus, when two parameters are known or assumed, the third parameter can be found. As a first step in describing the PSD of the fly ash found in suspension-firing of biomass, the PSD of corresponding samples of fuel and fly ash has been described by RR distributions, in order to examine the variations in the RR-parameters [Hansen et al., 2017a,b].

2.2.2. Rosin-Rammler Parameters

The parameters λ and n for a particle sample, can be determined from the cumulative distribution, by rearranging Equation [14] into Equation [16].

$$ln\left(-ln\big(1 - F(dp)\big)\right) = n \cdot \ln(dp) - n \cdot \ln(\lambda) \quad [16]$$

The cumulative function is linearized in Equation [16], and n and λ can be obtained by plotting ln(dp) against ln(-ln(1-F(dp))).

Examinations have been conducted for samples of wood and a straw fuels used in EFR-experiments by [Damoe et al., 2014]. In these experiments, corresponding samples of the ash were also analyzed. The RR-parameters obtained for the fuels, are listed in Table 2. In the table, calculated (from the fitted n and λ values), and, measured values of dp_{50} are also listed. It is seen that for the fuel samples examined, the exponent n is relatively constant (within 1,26-1,30), while the scale parameter, λ, varies with the median particle size of the sample. This is in line with findings by [Rosin and Rammler, 1933], who found that grinded coal samples most often have values of n within 1 to 1,35, while larger variation was found in the scale parameter [Hansen et al., 2017a,b].

Table 2: RR-parameters for fuels determined from 1 0-1 000 µm particles. PSD of the fuels were measured by [Damoe et al., 2014].

Particle sample	N	λ	R^2	$Dp_{50,calc}$ [µm]	$Dp_{50,meas}$ µm]
Straw	1.27	333	0.992	250	264
Wood	1.26	387.4	0.994	290	313
Wood[a]	1.30	387.7	0.990	292	309

a. Old wood fuel sample from similar experiments, included for comparison

The ashes from the straw and wood, produced from combustion in the EFR, have also been described by fitting RR-parameters to the measured PSD's. However, samples of the ashes collected had trimodal particle size distributions, which need to be considered. The three peaks appear at particle sizes (1) d_p < 1 µm, (2) d_p within 1 - 100 µm, and, (3) d_p > 200 µm. The measured PSDs of the ashes are seen in Figure 4. For further details, see [Damoe et al., 2014]. The RR-distribution, can only be applied to a single peak.

The cumulative distributions obtained by mathematical descriptions of different peaks, can then subsequently be combined, if necessary. However, only the intermediate peak is considered in this work. The peak occurring at d_p < 1 µm is considered to be aerosols of vaporized species (K, Cl and S), which is not considered as part of the coarse ash.

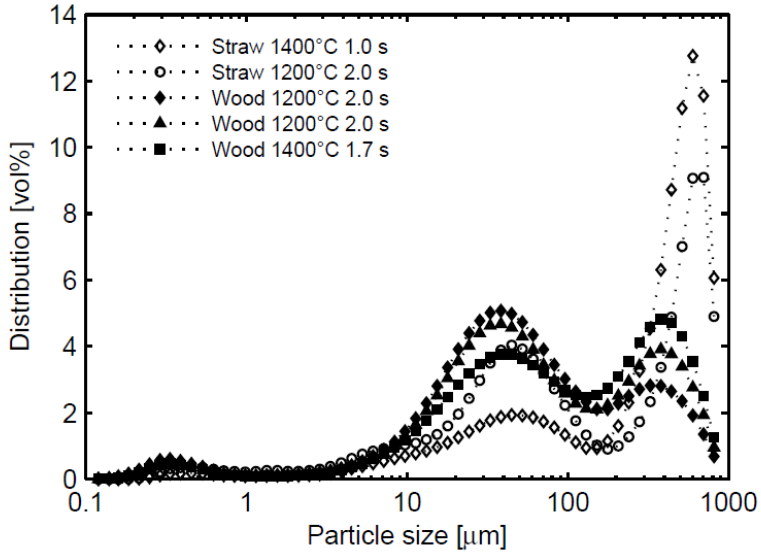

Figure 5: Measured particle size distributions of ashes from EFR experiments obtained at the given temperature and residence time. Data from [Damoe et al., 2014].

Table 3: RR-parameters for ashes obtained at different combustion temperatures of wood and straw. The RR-parameters and the measured dp50 are determined from the 1-15 0 μm particles. PSD of the ashes were measured by [Damoe et al., 2017].

Fuel	Res. T	Comb. Temp.	n	λ	R^2	Dp_{50}, calc	Dp_{50}, meas
	[s]	[°C]		[μm]		[μm]	[μm]
Wood[a]	2.0	1200	1.56	47	0.992	37	34
Wood[a]	2.0	1200	1.63	41	0.994	33	32
Wood	1.7	1400	1.58	42	0.994	34	33
Straw	2.0	1200	1.26	45	0.990	34	36
Straw[b]	1.0	1400	1.35	43	0.990	33	33

Note: a) Repetition of ash PSD measurement from the same ash sample, and, b) No sample from the full residence (1,7) time available.

The appearance of the fraction of large particles is unexpected and not yet understood [it is possibly particles with some degree of unburnt organic material, a hypothesis supported by chemical analysis]. The fraction of large particles accounts for 25-45 wt% of the ash samples [Hansen et al., 2017a,b].

The cumulative distribution seen in Figure 5 was recalculated to only contain particles within 1 and ~150 μm (the minimum between the peaks are determined for each particle sample), before fitting the RR-parameters to the distribution. In Table 3, the RR-parameters fitted to the fly ashes along with calculated (from the fitted n and λ), and, measured values of dp_{50} are listed.

It is seen that the PSDs of the ashes are relatively independent of combustion temperature in the range examined here. The PSD of the wood ashes seem to be more narrow than the PSD of the straw ashes, since the exponent n is higher for the wood ashes. The exponent of the straw ashes is close to the exponent of the fuels observed above.

In Figure 6, the PSD of ashes obtained at 1200 °C, are shown along with the fitted distributions. In the Figure a second distribution with a fixed exponent n = 1,30 is also shown, to examine the influence of choosing a fixed parameter to be used for all particle samples. By using a fixed parameter, the shape parameter λ is determined from Equation [15], with the measured dp_{50} and the fixed n value, as input.

It is seen that it is reasonable to assume a constant value of the exponent n = 1,30, to fit the ash PSD. Since both the fuel and ash samples examined here can be described by a RR-distribution with n ≈ 1,30, it seems that all particle sizes behave in a reasonable similar manner - i.e. with the same degree of coalescence or fragmentation. The same conclusion was obtained by [Sarofim et al., 85] for lignite and bituminous coal.

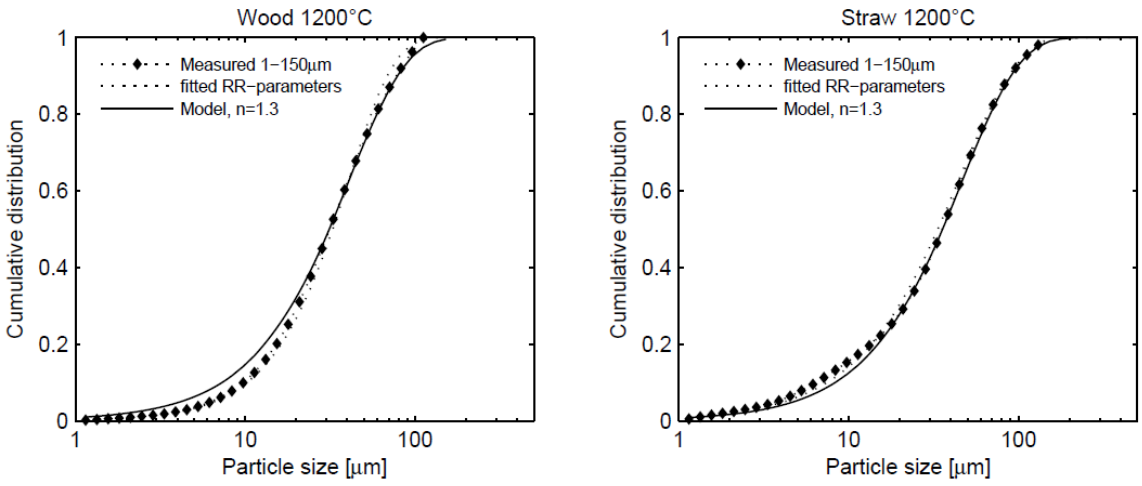

Figure 6: Measured PSD of wood ash (left) and straw ash (right) and PSD described by RR parameters fitted to the data and by a PSD described by a measured dp50 and the assumed n=1.3. Data from [Damoe et al., 2017]

Assuming n = 1,3 for all particle samples, a PSD can be described by using a measured or calculated dp_{50} along with the fitted value of n to calculate the scale parameter, λ, by Equation [15]. Below, it is described how the dp_{50} of the ash can be calculated from a median particle size (dp_{50}) of the fuel.

2.2.3. Ash Median Particle Size

In the ash formation model presented here, the particle size of an ash particle is calculated from the size of the 'parent' fuel particle, by taking the densities of fuel and ash into account along with the ash mass fraction of the fuel, and, the vaporization of K, Cl and S. Also, a parameter, describing possible breakage of the particle into a number of fragments is included [Hansen et al., 2017a,b].

Initially, the mass of a fuel particle is calculated.

$$m_{fuel} = \frac{1}{6} \cdot \pi \cdot \rho_{fuel} \cdot dp_{fuel}^3 \qquad [17]$$

The mass of an ash particle formed from the fuel particle, is then calculated, including the number of fragments formed by each particle, N_{frag}. If N_{frag} = 1, full coalescence of the ash within a fuel particle, is assumed. The ash fraction of the fuel is corrected for the vaporized species; K, Cl and S, which are not present in the particle for coalescence.

$$m_{ash} = \frac{m_{fuel} \cdot X_{ash} \cdot (1 - X_{vap})}{N_{frag}} \qquad [18]$$

Then, the diameter of ash particle size, originating from the fuel particle, is calculated.

$$dp_{ash} = \sqrt[3]{\frac{6 \cdot m_{ash}}{\pi \cdot \rho_{ash}}} \qquad [19]$$

The equations are combined:

$$dp_{ash} = \sqrt[3]{\frac{\rho_{fuel} \cdot X_{ash} \cdot (1 - X_{vap})}{\rho_{ash} \cdot N_{frag}}} \cdot dp_{fuel} \quad [20]$$

The number of fragments formed per particle have been calculated for the combus-tion experiments conducted by [Damoe et al., 2017], where corresponding samples of fuel and fly ash are available. This implies that corresponding values of dp_{50} of the fuel and ash are known and the vaporised fraction was furthermore quantified as part of the experiment. Therefore, Equation [20] can be solved for N_{frag}.

The densities of fuels and ashes has not been measured, and thus have to be assumed. The densities of the fuels are assumed based on measurements made for similar fuels with relevant particle sizes. The densities of the ashes are derived from the densities of the oxides in the ash, and, the ash composition. The densities used in the model are listed in Table 4.

Table 4: Assumed densities of fuels and ashes used in the model.

Density	Straw	Wood
ρ_{fuel} [kg/m^3]	1300	1400
ρ_{ash} [kg/m^3]	2700	3100

The number of fragments formed per fuel particle is for wood 3,2. For wood it is found that the correction of volatile inorganic matter has limited influence (N_{frag}=3,9 if all ash elements are included), since this fuel has a low content of K, Cl and S (X_{vap} = 0,17). For straw, the content of these elements is high (X_{vap} = 0,57) and a great difference in the calculated number of fragments is observed, when the vaporized species is included as ash (N_{frag}=8) or corrected for as vaporized elements (N_{frag}=3,4). This highlight the importance of correcting for the volatile content of the fuel particles. When the vaporized species are excluded, the number of fragments formed per particle from straw are in the same range as observed for wood, just above 3 [Hansen et al., 2017a,b].

The number of fragments calculated here, are in the same range as those calculated for lignite (N_{frag} = 3) and bituminous coal (N_{frag} = 5) by [Sarofim et al., 1977].

The model has been tested on particle size distributions provided by [Jiménes and Ballester, 2006]. Here, PSD was measured on three fuels (orujillo, chestnut wood and eucalyptus wood sawdust) and their ashes after combustion in an EFR [Hansen et al., 2017a,b].

2.2.4. Final Model for Ash PSD

In Figure 7, it is seen how the model performs in describing the particle size distribution of straw ash respectively wood ash, as measured by [Damoe et al., 2017]. In the figures, the PSD of the ash has been calculated by two methods; by the method described here, where the dp_{50} of the ash is calculated from the dp_{50} of the fuel (Equation [20]) and a Rosin-Rammler distribution is used to describe the distribution around the dp_{50} (Equations [14] and [15]). The second method in Figure 6 is a 'direct PSD calculation', where each particle size of the fuel PSD are used to calculate the resulting ash PSD (Equation [20]), assuming that the ash particles will account the same fraction of the total PSD as the parent fuel particles. In both calculation approaches, N_{frag} is set to 3, the densities shown in Table 4 are used, and X_{vap} is 0,17 for wood, and, 0,57 for straw. It is seen in Figure 7 that both calculation methods offers a good description of the PSD of the ash. The fit of the 'direct dp calculation' supports the assumption that all particles fragment to the same degree (for this range of particle sizes).

When parameters for the particle size distribution of the ash is determined (n and λ), the particle size distribution can be determined by a desired number of particle sizes. In the model,

as a first approach the PSD is described by 10 size-classes (N_{part}=10), each containing 10 wt% of the ash. To do this, Equation [14] is rearranged to calculate the particle sizes at which 10 %, 20%, 30%, etc. of the particles are below. To calculate 10 %, F(dp) = 0,1;

$$dp = exp\left[\frac{1}{n} \cdot \left(lm\left(-\ln\left(1 - F(dp)\right)\right)\right) + \ln(\lambda)\right] \quad [21]$$

As F(dp)= 1 cannot be used in Equation [21], the upper limit is set to F(dp) = 0,999. Once the particle sizes separating the size-classes are found, the mean particle size of each size class is found by the average particle size of each class [Hansen et al., 2017a,b].

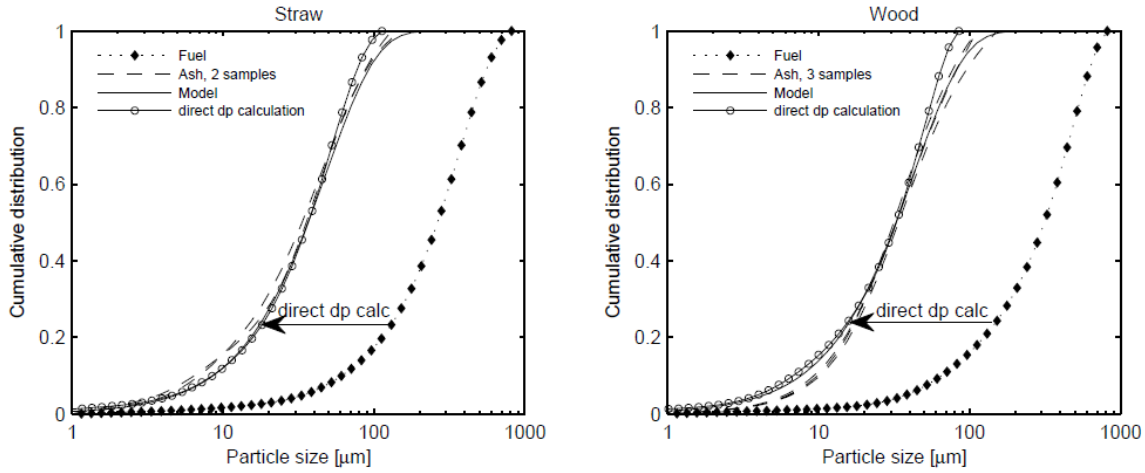

Figure 7: PSD model performance with Nfrag =3 and n=1,3. Xvap is 0,17 for wood and 0,57 for straw. Data from [Damoe et al., 2017]

2.2.5. Chemistry of the Coarse Ash Fraction

Both the concentration and also the chemical composition of the coarse ash fraction is important in the description of deposit formation. Though it has been observed that ash particles of different sizes do not have the same chemical composition, the coarse particles are in this model all assumed to have the same composition. The composition of the coarse ash particles are determined from the fuel ash chemical composition, which is corrected for the contents of the vaporized species. The molar fraction or mass fraction of each element-oxide in the ash is then recalculated to sum to 1.

3. Simulations of Aerosol and Fly Ash Formation

The above model were applied to simulate aerosol and fly ash formation for two of the fuels, fired in the entrained flow reactor at DTU, milled wood pellets and straw. The proximate and ultimate analyses of the fuels, are listed in Table 5, while the ash chemical analyses are listed in Table 6.

The straw sample analyzed has a very high Si-content, and a low content in both K and Ca, compared to normal straw analyses [Frandsen, 2011].

Table 5: Proximate and ultimate analyses of straw respectively milled wood pellets investigated in this study.

	Straw	Milled Wood Pellets
H_2O, %wt	7.32	5.87
Ash, %wt	10.83	1.11
Volatiles, %wt	65.38	79.86
Fixed C, %wt	16.47	13.17
C, %wt	41.75	47.96
H, %wt	4.85	6.65
O, %wt	34.09	38.20
N, %wt	0.61	0.10
S, %wt	0.24	0.07
Cl, %wt	0.51	0.03

Table 6: Ash chemical analyses [in %wt] of straw respectively milled wood pellets investigated in this study.

	Straw	Milled Wood Pellets
Al_2O_3	2.46	2.76
CaO	2.11	30.65
Fe_2O_3	0.72	1.53
K_2O	10.58	20.59
MgO	2.34	6.72
MnO		0.83
Na_2O	0.46	0.66
P_2O_5	0.35	2.83
SiO_2	73.39	19.30
TiO_2	0.09	0.17

3.1. Release of K,S and Cl: Freeboard Chemistry

For milled wood pellets, it can be seen that ([Ca]+[Mg])/Si > 0,5, which according to Eqn. (2) mean that 90 % of the K in this fuel is released, during combustion. In the case of straw, ([Ca]+[Mg])/Si < 0,5, and [K]/[Si] < 1, which means that the fraction of K released is equal to 0,48(K/Si)+0,42 = 0,51, i.e. that 51 % of the K will be released to the gas phase, the rest remaining in the coarse ash.

Based on this, $n_{Cl,vap}$, $n_{S,vap}$ and $n_{K,vap}$ are calculated for the two fuels:

Flux:	Straw	Milled Wood Pellets
$n_{Cl,vap}$	0.1439	0.0085
$n_{S,vap}$	0.0749	0.0218
$n_{K,vap}$	0.1324	0.0498

For the freeboard chemistry, > 900 °C, the molar fractions of KCl, K_2SO_4 and KOH is calculated by assuming global equilibrium in the system (FactSage). Below 900 °C, the frozen equilibrium model by [Christensen, 1995], eqns [9-12], is applied to determine [KCl] respectively [K_2SO_4]. By substituting eqns [10-12], a 3rd degree polynomial and be solved [HCl], from which [SO_2], [K_2SO_4] and [KCl] can then be determined.

3.2. Aerosol Formation

The temperature is reduced stepwise from 1350 °C, comparing in each step, pKCl, pK_2SO_4, and pKOH, the saturation temperature of the respective species, calculated from eqn. (13) applying the appropriate constants in Table 1.

Track is kept, simultaneously, on heterogeneous condensation of KCl, K_2SO_4, respectively KOH, assuming a uniform particle size of the coarse fly ash calculated from eqn (20), using the constants provided in Tables 3-4.

Eqn. (20) gives $D_{p,ash}$ = 63 µm for straw, respectively $D_{p,ash}$ = 28 µm for milled wood pellets.

If p_X/P_X^{sat} = 3, X∈{KCl, K_2SO_4, KOH}, at any point, nucleation of X is assumed.

For straw, K_2SO_4 nucleates homogeneously ~ 1165 °C, while for milled wood pellets, K_2SO_4 nucleates homogeneously ~ 1117 °C, below which temperatures the flue gas is quickly drained for KCl.

Assuming an aerosol size of 0,5 µm, the final aerosol mass loading is 196 mg/Nm^3 for straw and 63 mg/Nm^3 for milled wood pellets, see Table 7.

Table 7: Summary of aerosol simulations.

Fuel	**Straw**	**Milled wood pellets**
Nucleating species	K_2SO_4	K_2SO_4
Nucleating temperature	1165 °C	1117 °C
g aerosol/Nm^3	196	63
%wt KCl	32	11
%wt K_2SO_4	68	89

3.3. Coarse Fly Ash Formation

The size distribution of coarse fly ash particles were calculated, based on eqn (14), applying data from Tables 2-3. N_{frag} was set equal to 4, while n was set equal to 1,3 for straw and 1,5 for wood [Damoe et al., 2017]. Lambda was set equal to 43 µm for straw and 45 µm for milled wood. The coarse fly ash particles size distributions (PSDs) calculated are shown in Figure 8. Not much of a difference is observed in these PSDs.

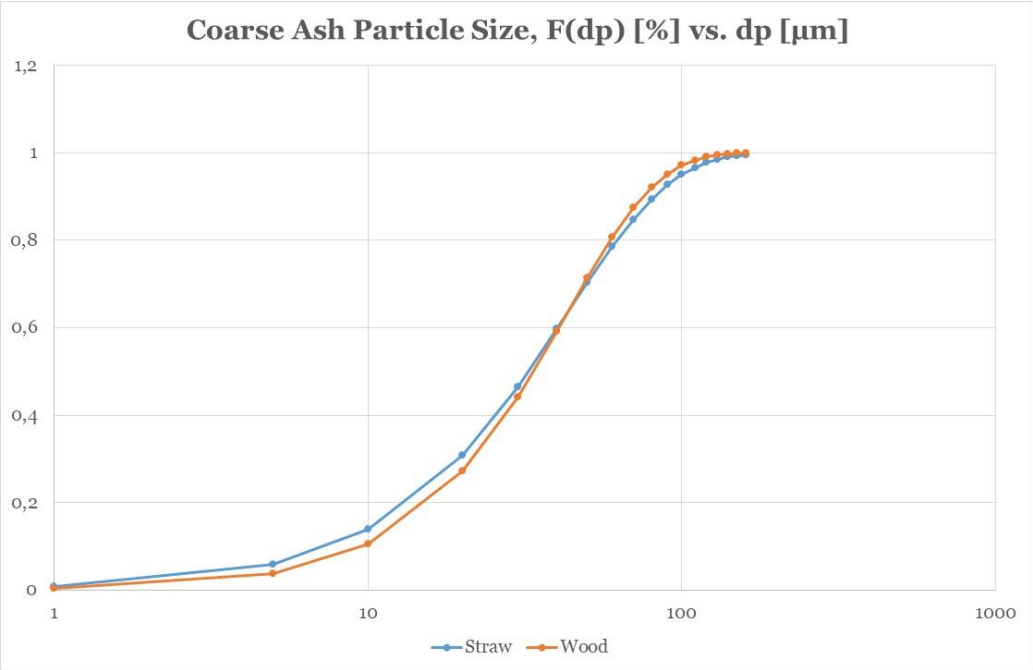

Figure 8: Calculated PSDS for straw respectively milled wood pellets, based on eqn (14).

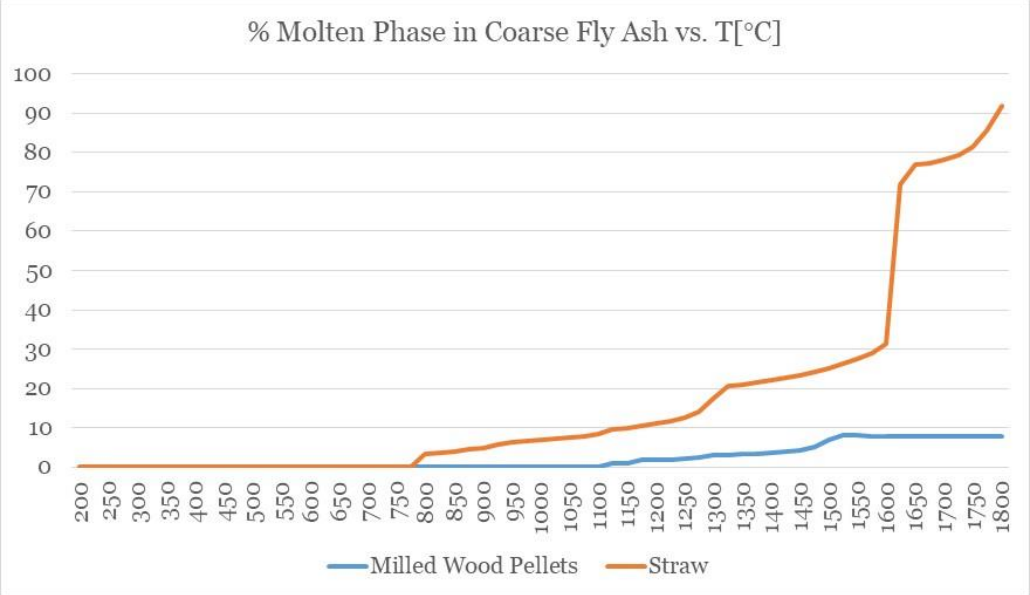

Figure 9: % molten phase in coarse fly ash particles

All K, which is not released to the gas to form aerosols, and left back in the coarse fly ash matrix. Global Equilibrium Analysis were done on the coarse fly ash composition for both straw and wood pellets. The percentage of molten phase in each of the two compositions are shown in Figure 9. It is seen that the coarse fly ash from straw, will be partly molten all the way down to 770 °C, while the coarse fly ash from milled wood pellets will be solid below 1120 °C. The amount of molten phase formed in the straw ash at 770 °C, depends strongly on the K/Si ratio in the ash. A higher K/Si-ratio would cause a higher fraction of molten phase.

The chemistry of the two coarse fly ashes was also calculated, see Figure 10.

Wood Pellets **Straw**

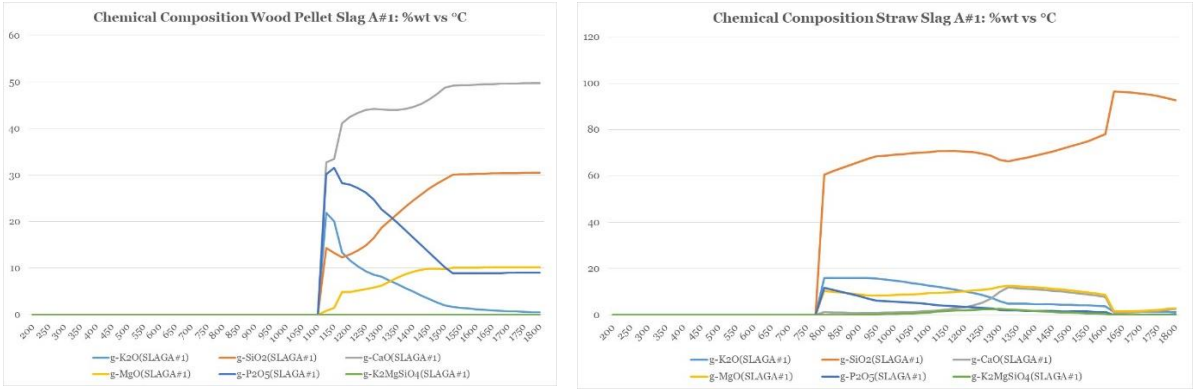

Figure 10: Chemical composition of molten phases formed in coarse fly ash particles from combustion of milled wood pellets respectively straw.

In Figure 10, it is seen that the molten phase in coarse fly ash from milled wood pellets is dominated by CaO, while SiO2 complete dominates the chemistry of the molten phase in the coarse fly ash from straw.

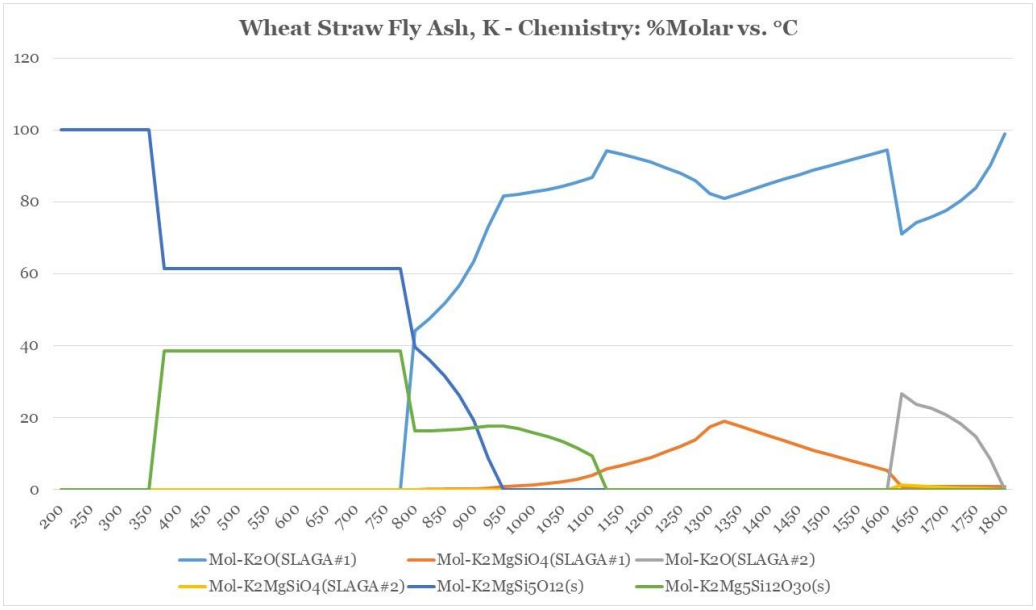

Figure 11: Overall chemistry of coarse fly ash from straw combustion, including both liquid and solid phases.

The coarse fly ash chemistry from straw is dominated by K-Mg silicate chemistry, below 800 °C.

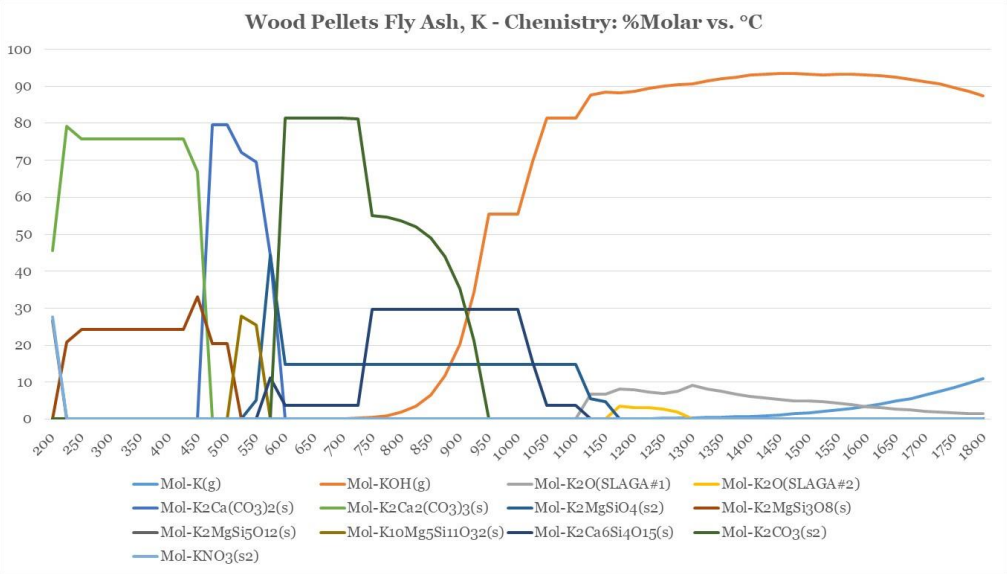

Figure 12: Overall chemistry of coarse fly ash from milled wood pellet combustion, including both liquid and solid phases.

The chemistry of the coarse fly ash from milled wood particles is, as seen in Figure 12, extremely complex. A lot more phases are stable in the ash compared to the coarse fly ash from straw.

4. Summary and Conclusion

Simulations have been conducted, based on a relatively simple engineering model, for aerosol and coarse fly ash formation, a model originally developed to supply the boundary conditions for a decent deposit prediction model.

As outlined above, a substantial number of assumptions and approximations have been made in the model. Nevertheless, the model provide reasonable estimates of mass loadings, as well as chemistries of aerosols and coarse fly ash particles, estimates that are in the range of expected values.

No comparison with actual particle sizes and chemistries have been made here, which serves merely to outline the frame and the capability of the model. But this comparison and thereby the merging between Biofficiency WPs 4 and 5 will be conducted, when this work is published, in the near future.

Considering the chemistry, Deliverable D4.2 already provided some detailed aerosol chemistry for comparison, while it should also be possible to compare the predicted coarse fly ash chemistry outlined here, with XRD-analyses of fly ash samples reported in Deliverable D4.1.

The most tricky thing at present is probably to combine the physical part of the aerosol and coarse fly ash formation with the needed equilibrium speciation of K-species, in the gas phase. This is currently done via transferring of tabulated data from FactSage to the aerosol/coarse fly ash model. An extremely time-consuming and tedious job. This will in a near future be built together via ChemApp.

The aerosol formation model could be improved. [Frandsen, 1995] presented a model for homogeneous nucleation of single species in cooling flue gases, based on a former MIT-work by McNallan et al., which could be combined with the coagulation model presented by [Christensen, 1995], and thereby provide a better estimate of both size distribution and chemistry of the aerosol.

Another aspect is the interface to advanced flow models (CFD), and thereby the prediction of deposit build-up, which is also to be addressed in the aftermath of Biofficiency.

Finally, the interaction between gaseous K-species and a potential additive, could be implemented, e.g. by assuming that the presence of the additive removes a certain amount of K from the flue gas, K which is then no longer available for e.g. heterogeneous condensation on entrained fly ash particles nor in formation of aerosols, upon cooling of the flue gas. Data for such capture is available both from the measurements conducted in Task 4.1 and via the work published by [Wang, 2018].

A future overall model, for both release, ash formation and deposition, may then appear as shown in Figure 13. The model work presented above, will be fitted into this scheme.

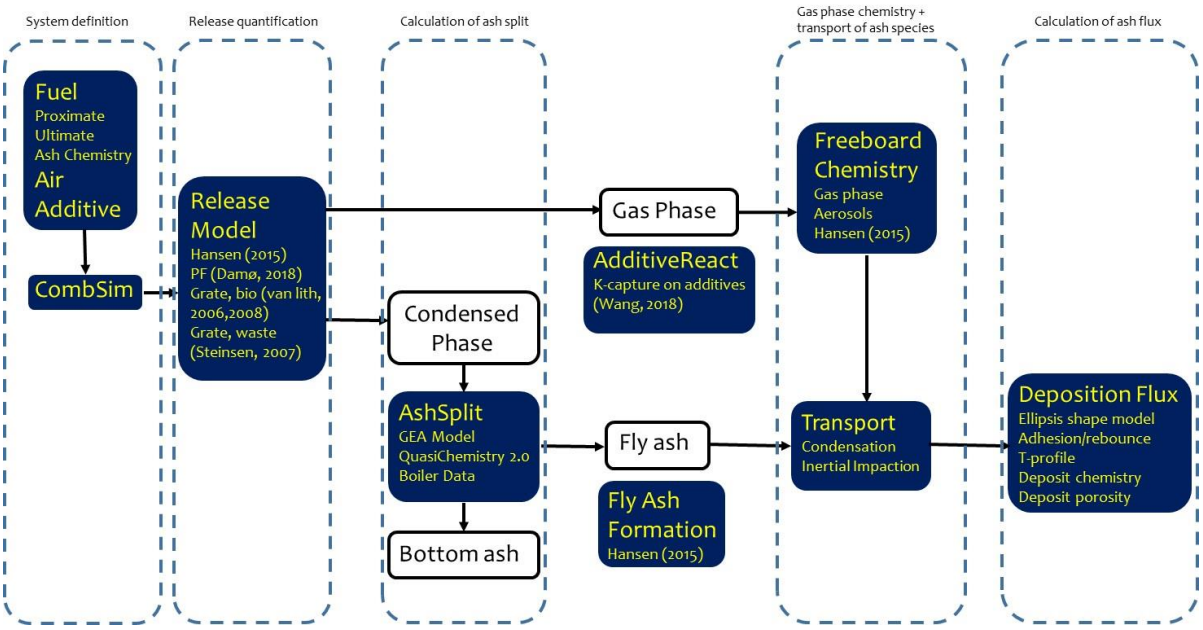

Figure 13: Overall model, for all aspects of ash and deposit formation.

References

Christensen KA, Stenholm M, Livbjerg H. The formation of submicron aerosol particles, HCl and SO2 in straw-fired boilers. J Aerosol Sci 1998;29:421-44.

Damoe, A. J.; Wu, H.; Frandsen, F. J.; Glarborg, P.; Sander, B. Impact of Coal Fly Ash Addition on Combustion Aerosols (PM2.5) from Full-Scale Suspension-Firing of Pulverized Wood. Energy Fuels 2014, 28, 3217−3223.

Damoe, A.J. ; Jensen, P.A. ; Frandsen, F.J.; Wu, H. ; Glarborg, P.; *Fly Ash Formation during Suspension-Firing of Biomass. Effects of Residence Time and Fuel-Type*; Energy & Fuels, 31(1), 555–570, 2017.

Frandsen, F.J.; Trace Elements from Coal Combustion; Ph.D.-Thesis, Dept. of Chem. Eng., DTU, ISBN 87-90142-03-9, 1995.

F.J. Frandsen; Ash Formation, Deposition and Corrosion When Utilizing Straw for Heat and Power Production; Doctoral Thesis, Technical University of Denmark, ISBN-9788792481405, 2011.

Frandsen, F.J.; Quantification of Release of Critical Elements, Formation of Fly ash and Aerosols: Status on Current Understanding and Research Needs; Proc. INFUB11, Albufeira, Algarve, Portugal, April, 18-21, 2017.

Hansen, S. B.; Jensen, P. A.; Frandsen, F. J.; Wu, H.; Bashir, M. S.; Wadenbäck, J.; Sander, B.; Glarborg, P. Deposit probe measurement in large biomass-fired grate boilers and pulverized-fuel boilers. Energy Fuels 2014, 28, 3539−3555.

Hansen, S.B., Jensen, P.A., Frandsen, F.J., Sander, B., Glarborg, P.; Mechanistic Model for Ash Deposit Formation in Biomass Suspension Firing. Part 1: Model Verification by Use of Entrained Flow Reactor Experiments; Energy and Fuels, 31(3), 2771–2789, 2017.

Hansen, S.B., Jensen, P.A., Frandsen, F.J., Sander, B., Glarborg, P.; Mechanistic Model for Ash Deposit Formation in Biomass Suspension-Fired Boilers. Part 2: Model Verification by Use of Full Scale Tests; Energy and Fuels, 31(3), 2790–2802, 2017.

Haynes, B. S.; Neville, M.; Quann, R. J.; Sarofim, A. F. Factors governing the surface enrichment of fly ash in volatile trace species. J. Colloid Interface Sci. 1982, 87, 266−278.

Helble, J. J. Mechanisms of ash particle formation and growth during pulverized coal combustion. Ph.D. Thesis, Department of Chemical Engineering, Massachusetts Institute of Technology, Cambridge, MA, 1987.

Jensen, P. A.; Frandsen, F. J.; Dam-Johansen, K.; Sander, B. Experimental Investigation of the Transformation and Release to Gas Phase of Potassium and Chlorine during Straw Pyrolysis. Energy Fuels 2000, 14, 1280−1285.

Jiménes, S., Ballester, J.; Particulate matter formation and emission in the combustion of different pulverized biomass fuels; Comb. Sci. techn., 178, 655-683, 2006.

Knudsen, J. N. Volatilization of inorganic matter during combustion of annual biomass. Ph.D. Dissertation, Department of Chemical Engineering, Technical University of Denmark, Kongens Lyngby, Denmark, 2004.

Knudsen, J. N.; Jensen, P. A.; Dam-Johansen, K. Transformation and release to the gas phase of Cl, K, and S during combustion of annual biomass. Energy Fuels 2004, 18, 1385−1399.

Korbee, R.; Shah, K. V.; Cieplik, M.; Betrand, C. I.; Vuthaluru, H. B.; van de Kamp, W. L. First line transformations of coal and biomass during pf combustion. Energy Fuels 2010, 24, 897−909.

Lighty JS, Veranth JM, Sarofim AF. Combustion aerosols: factors governing their size and composition and implications to human health. J Air Waste Manage Assoc 2000;50:1565-618.

Nordgren, D., Hedman, H., Padban, N., Boström, D., Öhman, M.; Ash Transformation in pulverized fuel co.combustion of straw and woody biomass; Fuel Processing Technology, 15, 52-58, 2013.

Sarofim, A. F.; Howard, J. B.; Padia, A. S. The Physical Transformation of the Mineral Matter in Pulverized Coal under Simulated Combustion Conditions. Combust. Sci. Technol. 1977, 16, 187−204.

Sarofim, A.F., Howard, J.B., Padia, A.S.; The physical transformation of the mineral matter in pulverized coal under simulated combustion conditions; Comb. Sci. Techn., 16, 401-412, 1977.

Shah, K. V.; Cieplik, M. K.; Betrand, C. I.; van de Kamp, W. L.; Vuthaluru, H. B. Correlating the effects of ash elements and their association in the fuel matrix with the ash release during pulverized fuel combustion. Fuel Process. Technol. 2010, 91, 531−545.

Rosin, P., Rammler, E.; The laws governing the fineness of powdered coal; The Inst. Fuel, 7, 29-36, 1933.

Vejahati, F.; Xu, Z.; Gupta, R. Trace Elements in Coal: Associations with Coal and Minerals and Their Behavior during Coal Utilization-A Review. Fuel 2010, 89, 904−911.

Wang, G.; *Potassium Capture by Kaolin and Coal Fly Ash*; PhD-Thesis, Department of Chemical and Biochemical Engineering, Technical University of Denmark, 2018.

Weibull, W.; A Statistical Distribution Function of Wide Applicability; ASMe Journal of Applied Mechanics, September, 293-297, 1951.

Wu, H.; Glarborg, P.; Frandsen, F. J.; Dam-Johansen, K.; Jensen, P. A.; Sander, B. Co-combustion of pulverized coal and solid recovered fuel in an entrained flow reactor − General combustion and ash behaviour. Fuel 2011, 90, 1980−1991.

Zheng, Y.; Jensen, P. A.; Jensen, A. D.; Sander, B.; Junker, H. Ash transformation during co-firing of coal and straw. Fuel 2007, 86, 1008−1020.